

Failure Mechanisms in Sand over a Deep Active Trapdoor

Yuri D. Costa¹; Jorge G. Zornberg, M.ASCE²; Benedito S. Bueno³; and Carina L. Costa⁴

Abstract: An experimental testing program was undertaken to investigate failure mechanisms induced by the active movement of a deep rectangular trapdoor underlying a granular soil. Reduced-scale models were tested under normal gravity as well as under an increased gravitational field using a centrifuge facility. Some models were used to evaluate the performance of both flexible and rigid pipes undergoing a localized loss of support. Failure mechanisms in the longitudinal direction of the models were characterized by a single, well-defined failure surface that developed within the limits of the trapdoor. However, failure mechanisms in the transverse direction of the models were characterized by multiple failure surfaces extending outside the limits of the trapdoor. Significant dilation of the soil located immediately above the trapdoor was identified in the failure of the models. The pattern of the failure mechanisms was found to be affected by the stress level and backfill density. Higher stress levels were found to lead to well-developed failure zones. The influence of backfill density was found to be more relevant in models involving flexible pipes. Pipes embedded within loose backfill were severely damaged after loss of support, while pipes embedded in dense backfill experienced negligible deformations. These results indicate that damage to pipelines caused by ground loss of support can be significantly minimized by controlling the compaction of the fill.

DOI: 10.1061/(ASCE)GT.1943-5606.0000134

CE Database subject headings: Failures; Arches; Buried pipes; Model tests; Sand, Soil type.

Introduction

The redistribution of stresses within the soil mass, often referred to as arching, has been analyzed using physical and analytical modeling of active and passive trapdoor systems (Terzaghi 1936; Koutsabeloulis and Griffiths 1989; Stone and Muir Wood 1992; Ono and Yamada 1993; Santichaiant 2002). The movement of an active trapdoor causes a reduction of soil stresses immediately above the trapdoor and an increase of stresses in the adjacent soil mass. The opposite trend has been observed in a passive trapdoor. The structure geometry, the soil properties, and the ratio between the height of soil cover and the width of the trapdoor (H/B) are the main variables that govern the trapdoor response.

Although good insight into the arching phenomenon has been obtained so far, an assessment of previous studies on the active trapdoor problem indicates that very limited information is available on the three-dimensional aspect of the problem, as most investigations have focused on plane strain and axis-symmetric conditions. While plane strain conditions can be assumed to as-

sess the performance of some geotechnical structures, this condition is not suitable for many problems, such as buried pipes.

Different responses have been reported for systems under deep and shallow conditions, which are characterized by soil cover ratios (H/B) over and below two, respectively (McNulty 1965; Koutsabeloulis and Griffiths 1989; Santichaiant 2002). However, the information available on failure mechanisms of trapdoor systems under deep conditions is very limited. The focus of previous studies on deep active conditions has been mainly on the variation of the loading over the trapdoor. Other aspects of the problem, including the analysis of failure mechanisms, have been generally overlooked.

The evaluation of buried pipes subjected to ground loss of support is an important application that can be analyzed by deep active trapdoor modeling under three-dimensional conditions. The demand for installation of deep buried pipelines has increased over the years, particularly in areas related to the oil industry and solid waste landfills (Yimsiri et al. 2004). Assessment of the three-dimensional nature of this problem is required to understand aspects of this problem related to the interaction of buried pipelines with the surrounding soil. Mining-related excavations, soil erosion due to pipe leaks, inadequate backfill compaction, and the presence of karstic soils are among the most usual causes that can trigger the ground loss of support.

Ground loss under pipelines is a complex soil-structure interaction problem that involves redistribution of stresses in the pipe wall as well as in the surrounding soil. The pipe may experience high circumferential and longitudinal bending moments in the vicinity of the void, which may eventually lead to structural failure. If the pipe is located at relatively high depth, additional problems may result from high thrust stresses that develop at the pipe wall (Katona 1988). In order to adequately address this problem, guidelines for the design of buried pipeline systems undergoing localized loss of ground support are needed.

This paper addresses perceived deficiencies by investigating the propagation and three-dimensional patterns of failure surfaces induced by an active, deep trapdoor underlying a granular soil

¹Professor, Dept. Civil Engineering, Federal Univ. of Rio Grande do Norte, Campus Universitário, Natal-RN, Brazil 59072-970 (corresponding author). E-mail: ydjcosta@ct.ufrn.br

²Fluor Centennial Associate Professor, Dept. Civil Engineering, The Univ. of Texas at Austin, 1 University Station, C1792, Austin, TX 78712-0280. E-mail: zornberg@mail.utexas.edu

³Professor, Dept. of Geotechnical Engineering, Univ. of São Paulo at São Carlos, Av. Trabalhador São-Carlense, 400, São Carlos-SP, Brazil 13566-590. E-mail: bsbueno@sc.usp.br

⁴Professor, Federal Institute of Education, Science and Technology of Rio Grande do Norte, Av. Salgado Filho, 1559, Natal-RN, Brazil 59015-000. E-mail: cmlins@gmail.com

Note. This manuscript was submitted on December 29, 2007; approved on April 22, 2009; published online on April 27, 2009. Discussion period open until April 1, 2010; separate discussions must be submitted for individual papers. This paper is part of the *Journal of Geotechnical and Geoenvironmental Engineering*, Vol. 135, No. 11, November 1, 2009. ©ASCE, ISSN 1090-0241/2009/11-1741-1753/\$25.00.

Table 1. Results from Previous Studies Involving Active Trapdoors in Granular Soil

Soil cover ratio (H/B)	Backfill properties			Target g -level	Trapdoor geometry	Recording technique	Reference
	D_{50} (mm)	D_r (%)	δ/B_{max} (%)				
1–5	0.44	N.R.	21	1	rectangular	photographic	Evans (1983)
1.65	0.33	N.R.	17	1	rectangular	photographic	Vardoulakis et al. (1981)
0.55	0.4, 0.85, 1.5	87	6	1, 100	rectangular	X-ray	Stone and Muir Wood (1992)
2	0.16	86	2	1	rectangular	photographic	Tanaka and Sakai (1993)
2	0.1	40	17	1, 75	circular	photographic	Santichaiainant (2002)
2	0.22	85	14	45	rectangular	photographic	Present study

Notes: D_{50} =mean particle size; D_r =relative density; δ/B_{max} =trapdoor maximum relative displacement; and N.R.=value not reported.

mass. The experimental program involved reduced-scale models prepared using dry sand and tested under normal gravity as well as under an increased gravitational field using a centrifuge facility. Some models involved the use of an aluminum tube resting over the trapdoor in order to evaluate the failure mechanisms of pipeline subjected to a localized loss of ground support. Emphasis of this study is placed on inspection of the kinematics of the problem and the effect of governing parameters such as stress level, backfill density, and pipe stiffness.

Previous Studies on Failure Mechanisms of Active Trapdoor Models

Table 1 summarizes the results from previous studies involving active trapdoor model tests in granular material. Only studies that included monitoring of the development of failure patterns within the backfill are summarized. Most of the available information is based on models built with soil cover ratios (H/B) equal to or below 2, which is the limit ratio below which an installation can be classified as shallow (Koutsabeloulis and Griffiths 1989; Sloan et al. 1990).

Fig. 1 shows a schematic representation of the typical failure mechanism reported in studies involving shallow conditions. A failure surface OA was typically reported to initiate from the corners of the trapdoor (point O) and to propagate toward the center of the trapdoor. The path followed by surface OA is defined by the soil density and its confinement, which are variables that govern the soil dilatancy. The angle formed between the vertical and the tangent at any point along surface OA equals the soil dilatancy

angle (ψ) that corresponds to that position at the time that the failure surface developed (Stone and Muir Wood 1992; Santichaiainant 2002).

The inclination of surface OA in the vicinity of point O is represented by θ_{i-OA} , which equals the soil dilatancy angle (ψ) at O . The failure surface OA propagates until point A once the trapdoor reaches a vertical displacement δ_1 (see Fig. 1). The failure surface has an inclination θ_{i-A} at this point, which corresponds to the dilatancy of the soil at A . Since the stress level at A is lower than that at O , the dilatancy angle at A is larger than that at O , and thus $\theta_{i-A} > \theta_{i-OA}$. The curved shape of the failure surface can be attributed to the effect on dilatancy of the varying overburden stress with depth.

The shear displacements that take place during development of the failure surface bring the soil along the failure zone to critical state and, consequently, ψ decreases from its initial value θ_{i-OA} , at the time of failure surface initiation, to zero for large trapdoor displacements. Specifically, continued vertical movement of the trapdoor has been reported to lead to the development of a new failure surface, shown as surface OB in Fig. 1, which propagates at an initial angle θ_{i-OB} . Since density of the soil in the vicinity of point O has decreased after development of the initial failure surface, the soil dilatancy decreased and surface OB forms an angle with the vertical that is smaller than that of surface OA (i.e., $\theta_{i-OB} < \theta_{i-OA}$). The failure surface propagates until point B once the trapdoor reaches δ_2 .

Radiographic data from physical models have shown that failure surface propagation switches from one discontinuity to the next in a relatively sudden manner, with the soil between the two failure surfaces remaining essentially as a rigid body and playing little role on the deformation process (Stone and Muir Wood 1992). Although the soil mass between two failure surfaces cannot be rigorously defined as rigid, this term is adopted herein for descriptive purposes.

The condition associated to a final trapdoor movement δ_3 can be represented by an approximately vertical failure surface, shown as surface OC in Fig. 1. For the final stage involving relatively large trapdoor movements, the soil can be assumed to have achieved critical state conditions, which is consistent with a negligible dilatancy and the development of a vertical failure surface.

The patterns of the failure surfaces develop within the soil mass due to an active trapdoor can be more complex than those illustrated in Fig. 1. Relevant factors that have been reported to affect these patterns include the soil density and stress confinement, which control the soil volumetric changes during shearing, as well as the soil particle size. A significant depression has been reported to occur on the ground surface directly above the trapdoor (Stone and Muir Wood 1992; Santichaiainant 2002).

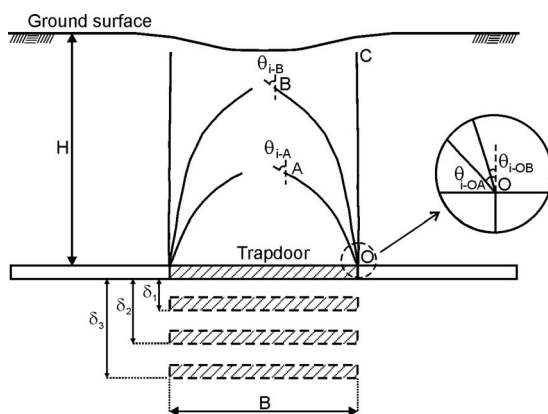


Fig. 1. Schematic view of the propagation of failure surfaces due to an active trapdoor under shallow conditions ($H/B \leq 2$)

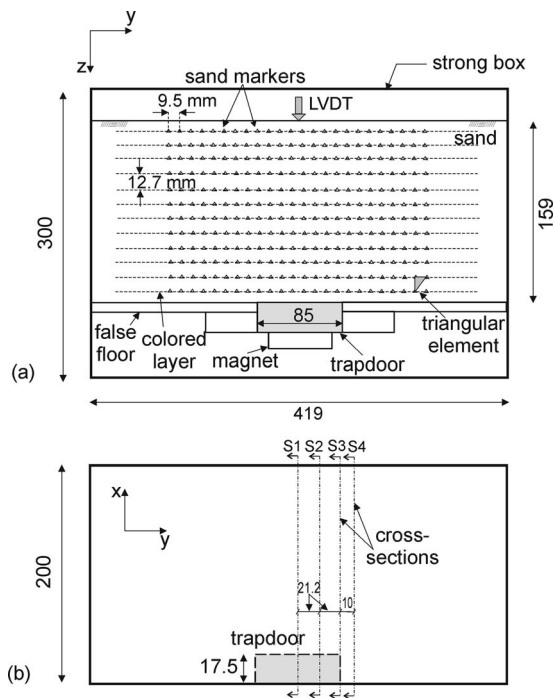


Fig. 2. Model configuration: (a) elevation view showing sand markers; (b) plan view showing position of the transverse sections within the backfill

Results from reduced-scale model tests conducted under deep conditions (Evans 1983) revealed failure mechanisms somewhat different from those found by other investigations for shallow conditions. Active trapdoor movements in models built with $H/B \geq 3$ led to a single failure surface that propagated from the corners of the trapdoor toward its center. Unlike the results reported in shallow model tests, which showed rigid zones of soil, the failure surfaces reported for deep conditions defined a soil zone above the trapdoor with significant dilation.

Active Trapdoor Model Tests

General Characteristics of the Models

Centrifuge modeling can be used to investigate specific phenomena, where the soil response is affected by the state of stresses, rather than to investigate the behavior of specific prototype structures. In this case, qualitative and quantitative information is obtained experimentally to validate or enhance the theories related to the phenomena under evaluation. In this investigation, centrifuge modeling was used to assess the role of the stress state, among other variables, on the behavior of systems where soil arching plays a significant role.

The models were constructed within a rigid aluminum strongbox with inside dimensions of 419×203 mm in plane and 300 mm in height. The strongbox and treatment of side walls are the same as those reported by Zornberg et al. (1998). Specifically, the front wall of the box consisted of a transparent Plexiglass plate used to enable visualization of the models during testing.

The elevation view of the model configuration and trapdoor setup used in this experimental investigation is shown in Fig. 2(a). The model includes an aluminum false floor with the same plane dimensions as the strongbox, where an aluminum trapdoor

fits. Fig. 2(b) presents the plan view of the model configuration, showing an aluminum trapdoor that was located against the Plexiglass wall and, consequently, it represents the half-section of a hypothetical rectangular trapdoor of length $L=85$ mm and width $B=35$ mm.

The reduced-scale models were tested in the 15-g-ton centrifuge at the University of Colorado at Boulder. This equipment is a Genisco 1230 rotary accelerator with a nominal radius of 1.36 m, and with capability of accelerating a 135-kg payload to an acceleration equivalent to 100 g (Ko 1988).

In order to achieve a homogeneous soil density, the models were prepared by pluviating air-dried sand into the strongbox. A 159-mm thick soil layer was used in all reduced models, which corresponds to a soil cover ratio H/B of 4.5. Downward vertical displacement of the aluminum trapdoor was triggered during testing by turning off the power of an electromagnet below the false floor. This caused the trapdoor to plunge with a predetermined vertical displacement δ , and creating a void within the soil mass.

The failure mechanism in the longitudinal section of the backfill against the Plexiglass wall was defined by monitoring the displacements of 12 thin layers of colored sand placed horizontally within the soil mass [Fig. 2(a)]. The colored layers included triangular discrete sand markers placed against the Plexiglass wall. This provided information useful to calculate strains within the soil mass induced by the trapdoor movement. The models were carefully wetted and dissected after testing in order to investigate the failure patterns in selected transverse sections within the backfill, identified as Sections S1–S4 in Fig. 2(b).

The settlement (s) of the soil surface was monitored in-flight after reaching the target g -level using a linear variable displacement transducer (LVDT) mounted on the top of the strongbox, immediately above the trapdoor. The rod of the LVDT was positioned at the center of the model (transverse Section S1), at a distance from the Plexiglass wall equal to $0.25 B$. Some models were tested using a second LVDT, also positioned in Section S1, but mounted at a distance of $1.2 B$ from the Plexiglass wall.

Image Collection and Analysis

Consecutive in-flight images were used to monitor the position of the colored sand layers along the transparent wall [y - z plane of the models, Fig. 2(a)]. After reaching the target g -level, images of the transparent wall were collected in flight before and after lowering the aluminum trapdoor. The images were collected from continuous videotape recording of the model tests.

The photographic method used in this study is based on that described by Zornberg and Arriaga (2003). Specifically, the image acquisition system consisted of a closed circuit camera and a video recording device. This system provided continuous monitoring of the models while testing was in progress. The resolution of the digitized images was $2,100 \times 2,800$ pixels.

Strains within the soil mass on the plane corresponding to the elevation view of the models (longitudinal section) were calculated from the collected images by tracking the coordinates of the center of mass of the sand markers. The sand markers defined the nodes of a mesh of 704 triangular elements that allowed calculation of the soil strains assuming linear transition of displacement in the domain [Fig. 2(a)].

The position of the colored layers in the transverse direction of the models (x - z plane) was photographically recorded using images of transverse sections that were collected after completion of each test. Four different sections [S1, S2, S3, and S4 in Fig. 2(b)] were used for this purpose.

Table 2. Summary of Conventional Triaxial Test Results with Ottawa F-75 Sand [after Batiste (1998)]

D_r (%)	σ'_3 (kPa)	ϕ'_p (°)	ϕ_{cr} (°)	ψ (°)	$(-d\varepsilon_v/d\varepsilon_a)_{max}$
87	68.9	42.4	35.5	15.4	0.79
87	34.5	44.8	37.0	15.4	0.80
88	11.2	44.6	37.9	15.2	0.98
84	1.3	48.0	34.3	24.6	1.43

Notes: σ'_3 =effective confining stress; ϕ'_p =peak friction angle; ϕ_{cr} =critical state friction angle; and ψ =dilatancy angle.

Backfill Properties

All reduced-scale models were prepared using dry Ottawa F-75 sand. This is a fine uniformly graded quartz (silica) sand that classifies as SP according to the Unified Soil Classification System. The sand has an average particle size of 0.22 mm, a coefficient of uniformity of 1.28, and a coefficient of curvature of 1.03. Its specific gravity is 2.65 and maximum and minimum void ratios are 0.805 and 0.486, respectively.

The shear strength parameters of the Ottawa sand, obtained from conventional triaxial compression tests, are presented in Table 2 (Batiste 1998). The results are reported for a soil relative density of approximately 85% and varying values of confining effective stress (σ'_3). Table 2 also includes the maximum dilatancy ratio $[-d\varepsilon_v/d\varepsilon_a]_{max}$ obtained at each confining effective stress.

Dilatancy ratio $(-d\varepsilon_v/d\varepsilon_a)$ versus ε_a curves obtained from the conventional triaxial tests conducted on Ottawa F-75 sand are shown in Fig. 3(a). These results show that the dilatancy ratio decreases significantly beyond ε_a of approximately 5% but it does not decrease to zero, at least for the range of strains used in these tests. Larger strains may be needed in order to attain critical state conditions.

Of particular importance is the effect of confining stress (σ'_3) on the sand volumetric behavior. Fig. 3(b) shows the variation of maximum dilatancy ratio with confining stress. The results show a very high maximum dilatancy for σ'_3 below 25 kPa and a comparatively smaller dilatancy for higher confining stresses. The soil volumetric behavior becomes nearly independent of confinement for σ'_3 higher than 50 kPa.

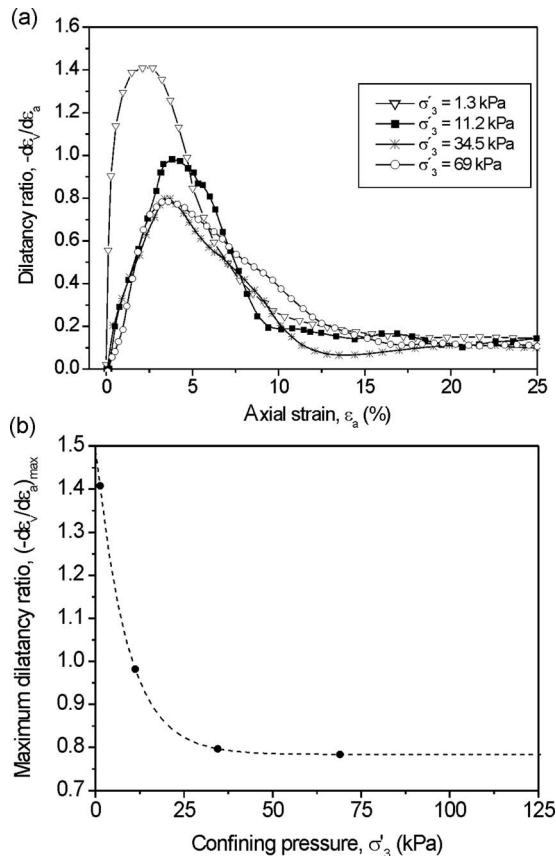


Fig. 3. Results of conventional triaxial tests on Ottawa F-75 sand [based on Batiste (1998)]: (a) dilatancy ratio versus axial strain curves; (b) maximum dilatancy ratio versus confining stress curves

Table 3. Summary of Model Tests

	Series A			Series B					Series C		Series D			
	A1	A2	A3	B1	B2	B3	BR ^c	BS ^d	C1	C2	D1 ^a	D2 ^a	D3 ^b	D4 ^b
Target g -level	45	45	45	1	1	1	1	1	45	1	45	45	45	45
Relative density, D_r (%)	85	85	85	85	85	85	85	85	42	42	85	42	85	42
Max. relative displacement, δ/B_{max} (%)	14	29	57	14	29	57	57	29	57	57	57	57	57	57

^aModel with rigid pipe.

^bModel with flexible pipe.

^cRepeated test.

^dModel with $H/B=2$.

Table 4. Characteristics of the Model Pipes

Pipe type	D_m (mm)	D_p (m)	t_m (mm)	t_p (mm)	EI_m (N m)	EI_p (kN m)
F	25.4	1.14	0.127	5.7	0.0123	1.12
R	25.4	1.14	0.7	31.5	2.06	187.5

the failure surfaces, Series A and B also included tests with trapdoor movements of 5 and 10 mm, which correspond to relative displacements of 14 and 29%, respectively.

Series B included one test to evaluate the repeatability of the results (Test BR) performed with the same characteristics of Tests B1, B2, and B3. The displacement of the trapdoor in Model BR was achieved in three continuous steps, corresponding to relative displacements of 14, 29, and 57%. The results obtained in the repeated test were essentially identical to those of Models B1, B2, and B3. Series B also included a “shallow” model, built with $H/B=2$ (Model BS). The failure mechanism obtained in Model BS was consistent with that reported in the literature for shallow conditions.

The tests in Series D were conducted with the objective of evaluating the influence of the presence of a pipe in the development of failure mechanisms due to active trapdoor movement. The model pipes used in these tests involved the half-section of aluminum tubes with smooth surface. The tubes were characterized by an outside diameter of 25.4 mm and a length of 400 mm. The wall thickness values, 0.127 and 0.7 mm, were selected to represent flexible and rigid pipes, respectively. Table 4 shows the characteristics of the model pipes. The subscripts m and p denote model and prototype, respectively, and EI represents the pipe flexural stiffness per unit length. The tube was placed against the transparent wall of the strongbox. Additional information on the experimental procedures and the testing program are provided by Costa (2005).

Evaluation of the Failure Mechanisms in the Longitudinal Section of the Models

Failure Mechanisms Overview

Fig. 4 shows the failure surfaces that developed along the longitudinal section (y - z plane), as observed from the Plexiglass wall. Results from Series A, performed under an acceleration of 45 g , are shown in Figs. 4(a–c). Also, results from Series B, conducted under normal gravity, are shown in Figs. 4(d–f). Fig. 4(a) shows the parameters used to describe the failure surfaces, which include the angle with the vertical of the initial portion of the failure surface (θ_i) and the maximum height of the failure surface measured from the base of the model (h_v).

The results in both series indicate that the downward movement of the trapdoor led to the development of a single failure surface at each corner of the trapdoor. The surface initiated at the corner of the trapdoor and developed toward the center of the model. Despite the large imposed trapdoor displacements, additional failure surfaces did not develop within the soil mass. The single failure surface that developed above the trapdoor is referred in this study as an internal failure surface.

The failure surface becomes more inclined to the vertical with increasing trapdoor movements as it propagates. That is, the angle between the initial portion of the failure surface at the corner of the trapdoor and the vertical (θ_i) gradually decreases with increasing trapdoor movements. This mechanism differs from that re-

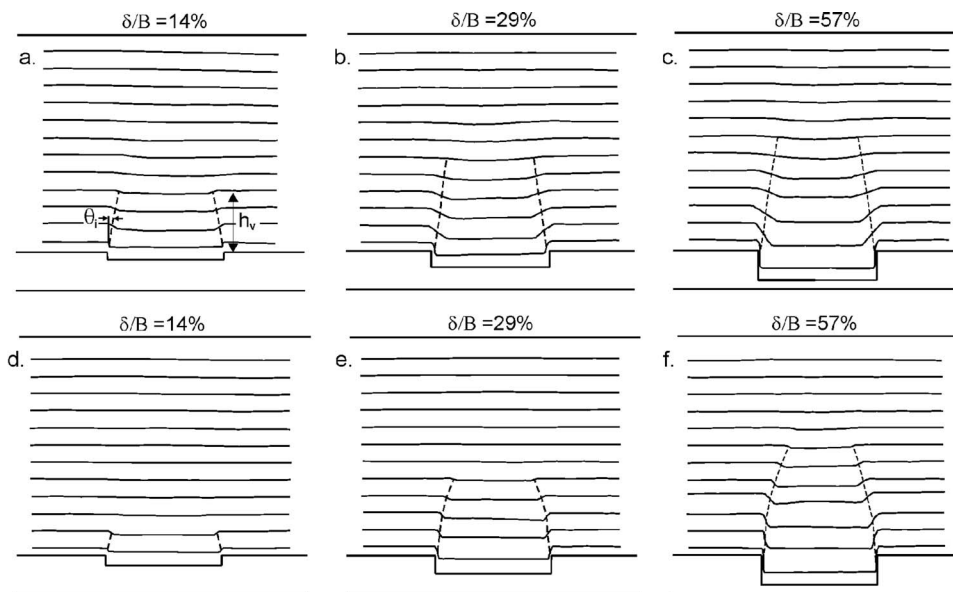


Fig. 4. Failure surfaces in the longitudinal section of models with dense backfill ($D_r=85\%$). Models tested under 45 g : (a) Model A1 ($\theta_i=9^\circ$); (b) Model A2 ($\theta_i=7^\circ$); and (c) Model A3 ($\theta_i=7^\circ$). Models tested under 1 g : (d) Model B1 ($\theta_i=13^\circ$); (e) Model B2 ($\theta_i=7^\circ$); and (f) Model B3 ($\theta_i=4^\circ$).

ported for shallow conditions, where successive failure surfaces with constant θ_i are obtained. Shearing in this case was reported to suddenly stop in the failure surface and to immediately continue in the subsequent one (Stone and Muir Wood 1992).

The angle (θ_i) was found to be lower for tests conducted under 45 g than for tests conducted under 1 g. For example, an inclination (θ_i) of 9° was measured at the corner of the trapdoor in the test conducted under 45 g for $\delta/B=14\%$ [Fig. 4(a)], but a comparatively larger inclination (θ_i) of 13° was obtained in the test conducted under normal gravity for the same relative displacement [Fig. 4(d)].

Under 1 g, an angle θ_i of nearly 7° was measured for a relative displacement $\delta/B=29\%$ and an even lower θ_i (4°) was measured at the relative displacement $\delta/B=57\%$. A similar trend was observed for increasing δ/B values in the tests conducted under 45 g, although the effect on θ_i is less significant at higher relative displacements.

The models tested under 45 g [Figs. 4(a–c)] resulted in comparatively larger failure surfaces, as quantified by the maximum height h_v , than in the models tested under normal gravity. The maximum height h_v , measured under 45 g equals approximately 1.2 B for a relative displacement of 14%. This height is about three times larger than that recorded under normal gravity for the same relative displacement. However, as the relative displacement increased, the failure surfaces under 1 and 45 g reached similar heights. Specifically, for a relative displacement of 57%, the failure surfaces developed both under 45 and 1 g reached a vertical height (h_v) of approximately 2.4 B. Overall, the influence of the applied g-level on the propagation of the failure surfaces was found to be more significant under low δ/B values.

The soil immediately above the trapdoor experienced dilation

due to the movement of the trapdoor, which is in agreement with the results reported by Evans (1983) for models with $H/B \geq 3$. In order to quantify the soil dilation in the region over the trapdoor, linear vertical strains (ϵ_z) were calculated for the tests conducted in Series A and B. The strains were calculated using data collected from images captured in the tests. Fig. 5 shows the contours of ϵ_z obtained using the initial and final coordinates of the markers recorded in the tests. The calculated lateral strains ϵ_y were significantly smaller than ϵ_z . Negative strains as shown in the contour labels correspond to volume increase. Since a reasonably symmetric response was observed in all tests, only results from one side of the models are shown in Fig. 5. The results show that soil dilation was more significant in tests conducted under 45 g than for tests conducted under normal gravity for a relative displacement (δ/B) of 14%. However, the effects of soil dilation become less significant for increasing values of δ/B . Additional contours from the other models are presented by Costa (2005).

Fig. 6 shows the failure surfaces recorded in the longitudinal section of the models prepared using loose backfills ($D_r=42\%$) and tested to a maximum relative displacement (δ/B) of 57% (Series C). The picture used to define the line art is also shown in Fig. 6. Failure surfaces with similar patterns were observed for tests conducted under 45 g and under normal gravity [Figs. 6(a and b), respectively]. The failure surfaces recorded in both models with loose sand were characterized by a height (h_v) equal to 1.8 B and an inclination to the vertical (θ_i) of 4°. This is an expected trend, since changes in dilatancy due to variations in confining stress are comparatively less significant in loose soil.

Influence of Soil Dilatancy on the Development of Failure Surfaces

The influence of soil dilatancy on the development of failure surfaces can be evaluated with the results of triaxial tests performed with the sand used as backfill in the centrifuge tests. The state of stresses in the soil surrounding the active trapdoor is complex and differs from the stress conditions imposed in triaxial tests. Yet, results from conventional triaxial tests can provide good insight into the data collected from the reduced scale models. Results of conventional direct shear and triaxial laboratory tests have also been used in previous studies of the trapdoor problem (Stone and Muir Wood 1992; Tanaka and Sakai 1993; Santichaianaint 2002; Muir Wood 2002). Moreover, the dilatancy ratio has been reported to be independent of the testing mode (Bolton 1986).

As observed for shallow conditions, the variations in the inclination of the failure surface in deep conditions are also associated to changes in soil dilatancy with shearing due to trapdoor movement. Conventional triaxial tests conducted with the sand used in

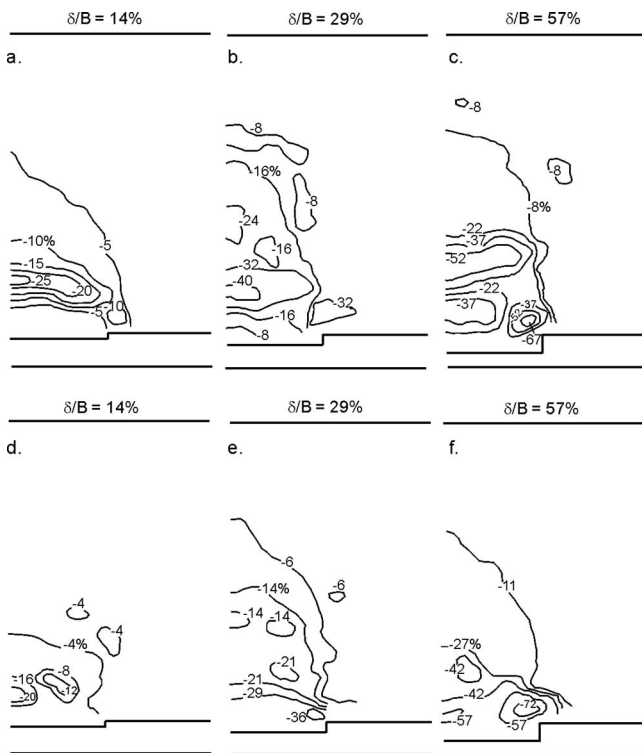


Fig. 5. Contours of vertical strains in the longitudinal sections of the models with dense backfill ($D_r=85\%$). Models tested under 45 g: (a) Model A1; (b) Model A2; and (c) Model A3. Models tested under 1 g: (d) Model B1; (e) Model B2; and (f) Model B3.

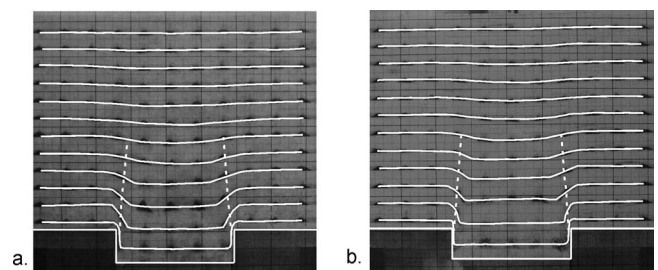


Fig. 6. Failure surfaces in the longitudinal section of models with loose backfill ($D_r=42\%$) for a relative displacement (δ/B) of 57%: (a) model tested under 45 g, (b) model tested under 1 g

this study for confining effective stresses (σ'_3) of 1.3 and 68.9 kPa led to maximum dilatancy angles (ψ) of 24.6 and 15.4°, respectively (Table 2). These confining stresses are similar to the mean initial stresses mobilized at the base of the models under 1 and 45 g, respectively. The initial portion of the failure surfaces in the model tests are expected to have developed with inclinations that are consistent with these values of dilatancy angle. When the trapdoor moves downwards, θ_i follows the decrease of ψ and reaches the values reported in Fig. 4.

The value reached by the dilatancy ratio ($-d\epsilon_v/d\epsilon_a$), of approximately 0.2 at large strains [Fig. 3(a)], corresponds to a dilatancy angle (ψ) of approximately 5°. This magnitude of dilatancy angle is consistent with the recorded angles (θ_i) of the initial portion of the failure surfaces, obtained at the relative displacement δ/B of 57% (i.e., 4° under 1 g and 7° under 45 g). This level of relative displacements induces large strains in the soil mass above the trapdoor. The good comparison between these results provides good evidence that initial inclination of the failure surface (θ_i) corresponds to the dilatancy angle (ψ) of the soil.

The dilatancy results obtained from the triaxial tests shown in Fig. 3 can also be used to clarify aspects of the failure patterns recorded in the longitudinal section of the models, related to the variation of θ_i with δ/B and the shape of the failure surfaces. The larger variations in θ_i with δ/B observed under 1 g [Figs. 4(d–f)] than under 45 g [Figs. 4(a–c)] can be explained by the larger variations in soil dilatancy from peak to residual values under lower stress levels than under higher stress levels. Moreover, unlike the curved failure surfaces obtained under 1 g [Figs. 4(d–f)], the nearly straight failure surfaces developed under 45 g [Figs. 4(a–c)] can be explained by the smaller variations in dilatancy under high confining stresses than under low confining stresses as shown in Fig. 3(b). The initial vertical effective stresses (σ'_v) in the models tested under 45 g varied from zero at the surface to 124 kPa at the base of the model, with the failure surfaces propagating in a region with σ'_v ranging from approximately 50–124 kPa. As shown in Fig. 3(b), changes in soil dilatancy with confining stress are minor within this range of stresses, which is consistent with the development of nearly straight failure surfaces.

Thickness of Failure Surfaces

The thickness of the failure surface (t) has been generally accepted to be on the order of 10 times the mean particle size of the soil (D_{50}) (Roscoe 1970). Muir Wood (2002) compiled t/D_{50} ratios from different experimental conditions and reported t/D_{50} ratios ranging from 7.3 to 18.5. Experiments involving active trapdoors with soil cover ratios H/B ranging from 0.5 to 2, have led to t/D_{50} values ranging from 10 to 21 (Vardoulakis 1981; Santichaiant 2002).

Table 5 summarizes t/D_{50} ratios measured in the longitudinal section of the models tested as part of this investigation. With the exception of the tests conducted using dense backfills ($D_r = 85\%$) under 1 g (Series B), the measured t/D_{50} ratios listed in Table 5 exceeded the value of 30, which is larger than typical ratios reported in the literature for shallow conditions.

The results also show that the thickness of the failure surfaces increased with increasing trapdoor relative displacement (δ/B) as shown in Table 5 for Series A and B (models with dense backfill under 45 and 1 g, respectively). This is consistent with findings reported by Scarpelli (1981) and Hartley (1982) based on direct shear test results. As the soil in the region of the failure surface is sheared, dilatancy decreases and some of the surrounding soil

Table 5. Thickness Ratios (t/D_{50}) of Failure Surfaces

Model	D_r (%)	g-level	δ/B (%)	t/D_{50}
A1	85	45	14	34
A2	85	45	29	62
A3	85	45	57	78
B1	85	1	14	16
B2	85	1	29	22
B3	85	1	57	29
C1	42	45	57	73 ^a
C2	42	1	57	67 ^b

^amin.(t/D_{50})=47 and max.(t/D_{50})=100.

^bmin.(t/D_{50})=27 and max.(t/D_{50})=107.

particles get involved in the deformation process. The failure surfaces that developed in loose backfill were comparatively wider than those developed in dense backfill.

Evaluation of the Failure Mechanisms in the Transverse Sections of the Models

Characteristics of the Failure Zones

Failure surfaces triggered by active trapdoors may also develop beyond the vertical failure surface OC shown in Fig. 1. As schematically illustrated in the transverse section shown in Fig. 7, larger trapdoor displacements would lead to the development of surfaces OD and OE, which propagate toward the mass of soil beyond the trapdoor. These failure surfaces develop due to the instability of the adjacent soil mass, which is mobilized by the continuous migration of soil into the underlying void. Since soil dilatancy decreases with increasing trapdoor displacement (δ) due to the significant shearing of the soil in the vicinity of point O, the angle with the horizontal of the initial portion of surface OE (θ_{e-OE}) is smaller than the angle of OD (θ_{e-OD}). Continued trapdoor movement is expected to cause the development of additional failure surfaces until reaching the limit surface OF, which is inclined with an angle θ_{e-OF} to the horizontal. The inclination of

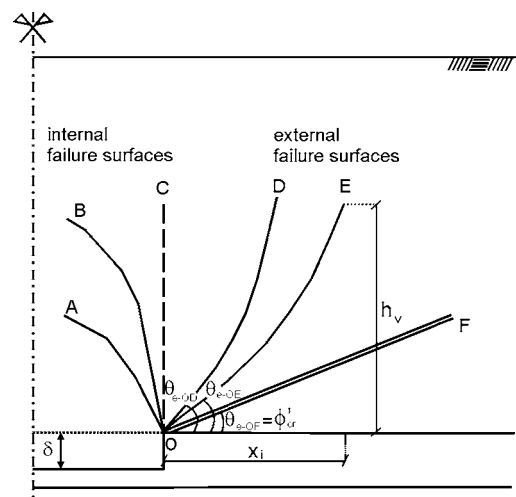


Fig. 7. Transverse section showing schematic view of development of internal and external failure surfaces in a soil mass above an active trapdoor

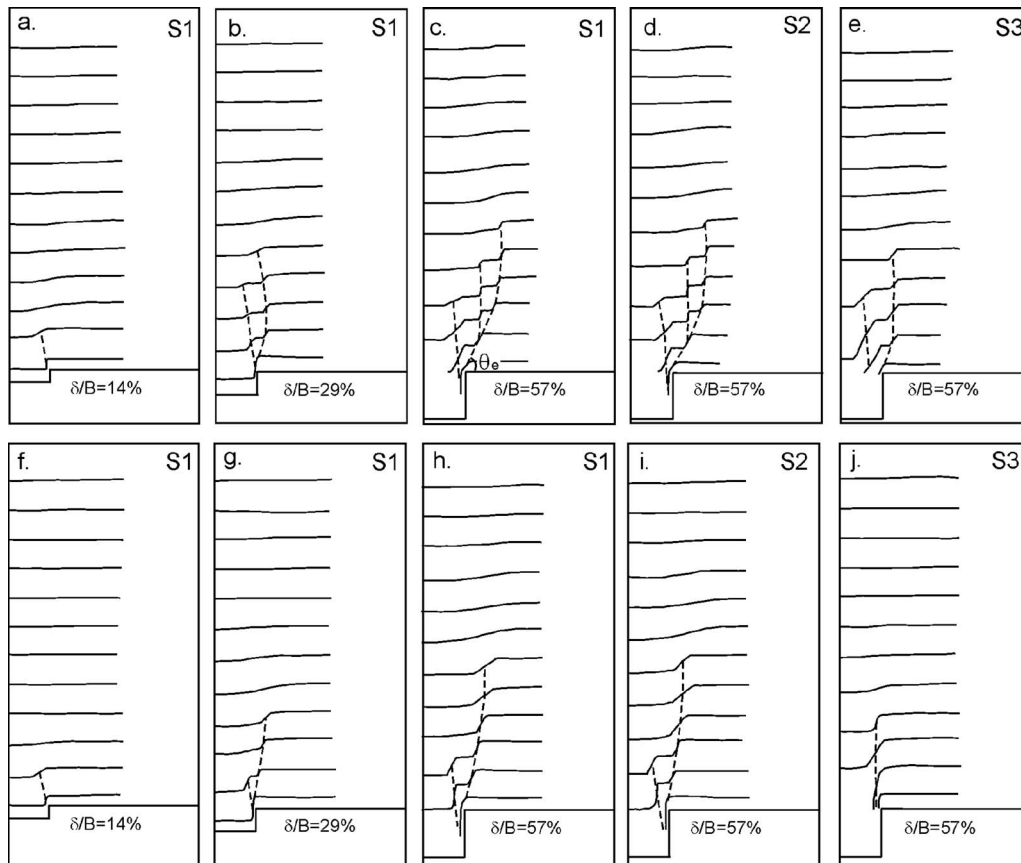


Fig. 8. Failure surfaces in transverse sections of models with dense backfill ($D_r=85\%$). Models tested under 45 g: (a) Model A1 (Section S1); (b) Model A2 (Section S1); (c) Model A3 (Section S1); (d) Model A3 (Section S2); and (e) Model A3 (Section S3). Models tested under 1 g: (f) Model B1 (Section S1); (g) Model B2 (Section S1); (h) Model B3 (Section S1); (i) Model B3 (Section S2); and (j) Model B3 (Section S3).

OF equals the angle of repose of the soil, which corresponds to the critical state friction angle (ϕ_{cr}), that represents the angle of shearing resistance of soil at its loosest state.

For the purposes of this study, failure surfaces developing within the limits of the trapdoor are defined as internal failure surfaces, while surfaces developing outside the limits of the trapdoor are defined as external failure surfaces. Thus, OA and OB in Fig. 7 represent internal surfaces, while OD, OE, and OF represent external surfaces. External failure surfaces correspond to the ultimate state of the active arching process. The development of external failure surfaces was originally envisioned by Terzaghi (1943), who indicated that the failure planes that develop due to an active trapdoor should extend beyond the width of the structure. This hypothesis was later confirmed experimentally by small scale model tests conducted for H/B values ranging from 2 to 5.3 (Ladanyi and Hoyaux 1969; Santichaiant 2002).

The failure surfaces that developed in the transverse sections ($x-z$ plane) of the models tested in this study to low trapdoor relative displacements (δ/B) were similar to those recorded in the longitudinal section ($y-z$ plane). That is, a single internal failure surface developed from the corner of the trapdoor. The internal failure surface was found to become gradually vertical (i.e., with lower θ_i) with increasing trapdoor movement. Ultimately, external failure surfaces developed for comparatively larger trapdoor movements.

Figs. 8(a–c) show the development of failure surfaces in transverse Section S1 ($x-z$ plane) in tests conducted using dense backfill ($D_r=85\%$) under an acceleration of 45 g (Series A). Figs.

8(f–h) show the failure surfaces obtained in transverse Section S1 also in tests conducted using dense backfill but under normal gravity (Series B). Different patterns of external failure surfaces were observed in the models tested under different g -levels. As can be seen in Fig. 8(c), conducted under 45 g, an internal and two external failure surfaces developed for a relative displacement (δ/B) of 57%, with the outermost external failure surface propagating as a bifurcation of the previous one. On the other hand, a single external failure surface was observed under normal gravity for the same relative displacement [Fig. 8(h)].

Table 6 summarizes the geometric characteristics of the failure zones recorded in transverse Section S1 of models tested using dense backfills (Models A3 and B3) and loose backfills (Models C1 and C2) for a relative displacement (δ/B) of 57%. The magnitude x_i reported in Table 6 is the length of the horizontal projection of the outermost failure surface measured from the corner of the trapdoor (see Fig. 7). As will be discussed in the next section, Table 6 also includes the results obtained with models that included pipes (Series D). The results in Table 6 indicate that models with loose backfills resulted in comparatively wider failure zones. Specifically, values of x_i measured in models constructed using loose backfill were nearly three times higher than those recorded in models with dense backfill. Since the ability of the soil to dilate decreases with increasing confinement, the external failure surfaces follow a less steep path when propagating in tests conducted under 45 g than those conducted under 1 g, resulting in comparatively wider failure zones.

Figs. 8(d and e) show the patterns of failure surfaces obtained

Table 6. Characteristics of Failure Surface Patterns in the Transverse Section S1 of the Models

	Model	D_r (%)	g-level	Pipe type	θ_e ($^\circ$)	x_i/B	h_v/B
Tests without pipe	A3	85	45	—	63	0.4	1.8
	B3	85	1	—	75	0.2	1.8
	C1	42	45	—	42	0.6	1.2
	C2	42	1	—	48	0.6	1.9
Tests with pipe	D1	85	45	Rigid	54	0.8	2.0
	D2	42	45	Rigid	43	0.8	1.9
	D3	85	45	Flexible	63	0.6	2.0
	D4	42	45	Flexible	44	0.8	1.6

in transverse Sections S2 and S3, respectively, in models of Series A (45 g). Similarly, Figs. 8(i and j) show the patterns obtained from the case of models of Series B (1 g) in the same transverse sections. The locations of transverse Sections S1, S2, and S3 are indicated in Fig. 2(b). The patterns of the failure surfaces observed in transverse Sections S1 and S2 are very similar. However, the patterns in transverse Section S3 revealed less developed failure surfaces, differing significantly from those recorded in the other two sections. A similar trend was observed in models constructed using loose backfill. The less developed failure surfaces near the corners of the trapdoor (transverse Section S3) is due to

the friction mobilized between the soil moving into the trapdoor and the soil outside the trapdoor region that remains stable.

The differences between the failure patterns observed in the longitudinal (y) and transverse (x) directions of the reduced-scale models can be explained by the difference in the trapdoor dimensions in these two directions with respect to the imposed trapdoor displacement (δ). For example, external failure surfaces did not develop in the longitudinal direction (y) of the models because the maximum trapdoor displacement (δ) was comparatively small in relation to the trapdoor length (L). On the other hand, the magnitude of δ was comparatively large in relation to the trapdoor width B , and triggered the development of external failure surfaces in the transverse direction (x) of the models.

Figs. 9(a and b) show the maximum height of the failure surfaces (h_v) as a function of the trapdoor displacement δ , recorded in the longitudinal section as well as in the transverse S1 section of models of Series A (conducted under 45 g) and Series B (conducted under 1 g), respectively. The values of h_v and δ were normalized by the corresponding trapdoor dimension in the plane under consideration (B or L). The figures show that the maximum height h_v of the failure surfaces developed in both longitudinal and transverse sections tend to follow a single trend with increasing trapdoor displacement δ . This result indicates that the differences in the failure mechanisms observed in both transverse and longitudinal directions are due to dimensional effects of the trapdoor.

Surficial Settlements

Table 7 summarizes the surficial settlement values (s) obtained on transverse Section S1. Settlements were recorded using LVDT's positioned at horizontal distances of $0.25 B$ (settlement $s_{0.25}$) and $1.2 B$ (settlement $s_{1.2}$) from the Plexiglass wall of the strongbox.

The soil relative density (D_r) significantly influenced the mag-

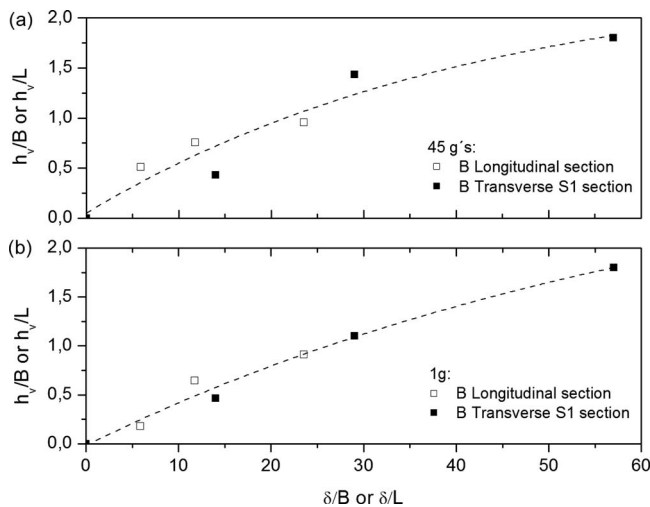


Fig. 9. Maximum height of failure surface (h_v) as a function of the trapdoor displacement δ , recorded in the longitudinal section and in the transverse S1 section of models: (a) Models tested under 45 g (Series A); (b) models tested under 1 g (Series B)

Table 7. Surficial Settlements on Transverse Section S1

	Model	D_r (%)	g-level	$s_{0.25}/\delta$ (%)	$s_{1.2}/\delta$ (%)	s_{max}/δ (%)	w/B
Tests without pipe	A1	85	45	6.7	4.0	6.9	5.9
	A2	85	45	5.1	3.0	5.2	5.9
	A3	85	45	4.8	3.0	4.9	6.1
	B3	85	1	0.0	0.0	0.0	0.0
	C1	42	45	13.6	—	—	—
	C2	42	1	6.4	—	—	—
Tests with pipe	D1	85	45	5.5	—	—	—
	D2	42	45	16.0	—	—	—
	D3	85	45	5.5	—	—	—
	D4	42	45	18.0	—	—	—

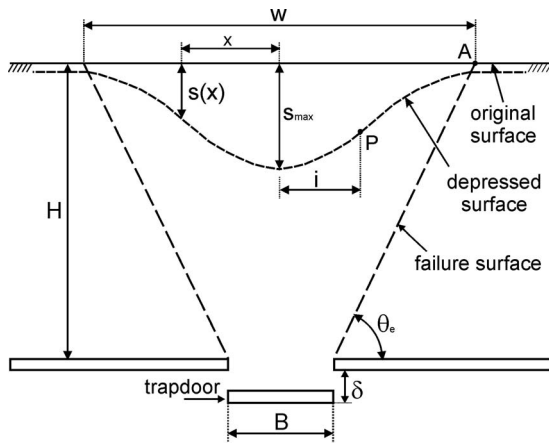


Fig. 10. Characteristics of surficial settlements

nitude of the surficial settlements. In spite of the deep conditions of the tests ($H/B=4.5$), larger surficial settlements were recorded on models with loose backfills ($D_r=42\%$) than on those with dense backfills ($D_r=85\%$). In general, surficial settlements were approximately three times larger in tests conducted using loose backfill. The stress level also played a significant role on surficial settlements, with models tested under an acceleration of $45\ g$ experiencing comparatively larger surficial settlements than models tested under normal gravity.

Of particular importance for the assessment of potential damages caused by underground openings in different subsoil conditions is the quantification of the maximum settlement (s_{max}) and the width (w) of the surficial depression. These parameters were quantified for the transverse section of those models where settlements in two positions ($s_{0.25}$ and $s_{1.2}$) were monitored during testing.

Consistent with empirical observations of surficial settlements induced by excavations of tunnels (Peck 1969), the surficial depression developed after lowering the trapdoor was assumed to be defined by a Gaussian distribution function, as follows:

$$s_x = s_{max} \exp[-0.5(x^2/i^2)] \quad (1)$$

where s_{max} =maximum settlement; i =horizontal distance measured from s_{max} to the inflection point P in the depression surface; x is the horizontal distance measured from the center of the depression to the point where settlement is measured; and w is the width of the depression (see Fig. 10). The failure zone in Fig. 10 is represented by straight external failure surfaces emerging from the corner of the trapdoor and intersecting the surface of the soil at point A . Based on the geometry shown in Fig. 10, the angle to the horizontal (θ_e) of the external failure surface equals

$$\theta_e = \tan^{-1}[2H/(w - B)] \quad (2)$$

The width of the depression (w) is given by

$$w = 2i(2\pi)^{1/2} \quad (3)$$

The predicted s_{max} and w values using Eqs. (1) and (3) are shown in Table 7 for those models where settlements in two positions were measured on transverse Section S1. The measured values $s_{0.25}$ and $s_{1.2}$ were used as input parameters to obtain s_{max} and i using Eq. (1), and the width w was then obtained using Eq. (3). The predicted width values for models of Series A were about six times larger than the trapdoor width.

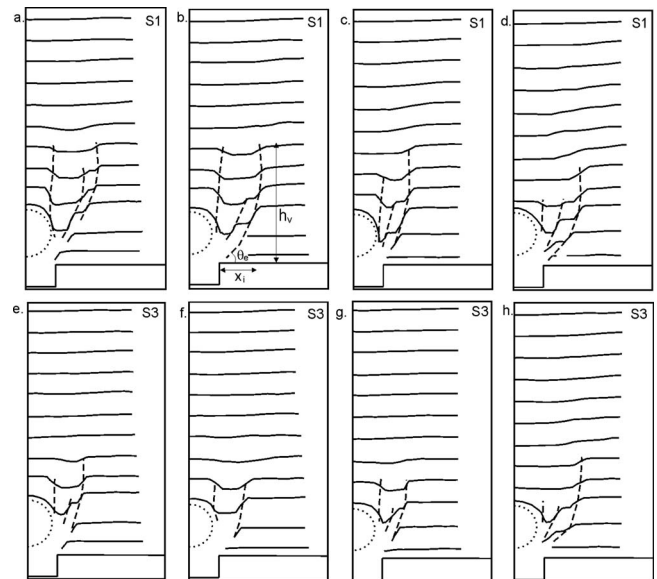


Fig. 11. Failure mechanisms recorded in models containing pipes tested under $45\ g$ to a relative displacement (δ/B) of 57% . Section S1: (a) rigid pipe in dense backfill (Model D1); (b) rigid pipe in loose backfill (Model D2); (c) flexible pipe in dense backfill (Model D3); and (d) flexible pipe in loose backfill (Model D4). Section S3: (a) rigid pipe in dense backfill (Model D2); (b) rigid pipe in loose backfill (Model D3); and (c) flexible pipe in dense backfill (Model D3); and (d) flexible pipe in loose backfill (Model D4).

The inclination of the initial portion of the external failure surface in transverse Section S1 in Models A2 and A3 was predicted using Eq. (2) considering the corresponding width w obtained from Eq. (3) and the cover ratio $H/B=4.5$. The predicted θ_e values equal 77° and 60.5° for Models A2 and A3, respectively. These results compare very well with the experimentally obtained values, which equal 75° and 63° for Models A2 and A3, respectively.

Failure Mechanisms Involving Buried Pipes Subjected to Ground Loss

The study of failure mechanisms induced by active trapdoors is of particular relevance in cases involving the presence of pipelines within the soil mass. Fig. 11 shows the failure patterns observed in transverse Sections S1 and S3 for Series D models, which were constructed as the models in the previous series, but including an aluminum tube with outside diameter of $25.4\ \text{mm}$. All models were tested under $45\ g$. As shown in Figs. 11(a-d), the recorded failure patterns showed three distinct failure surfaces propagated from the corner of the trapdoor. The innermost of the three surfaces developed due to the sliding of the soil besides the pipe into the underlying void. The other two failure surfaces are external failure surfaces and developed from subsequent instability of the soil mass next to the trapdoor in an attempt to fill the void created by the trapdoor movement. The outermost failure surface propagated into the soil mass at an initial angle θ_e and subsequently became nearly vertical after reaching the elevation of the pipe crown. The characteristics of the models in the D Series and of the failure zones are provided in Table 6.

Figs. 11(e-h) show the failure patterns recorded in transverse Section S3 of the Series D models. Consistent with results ob-

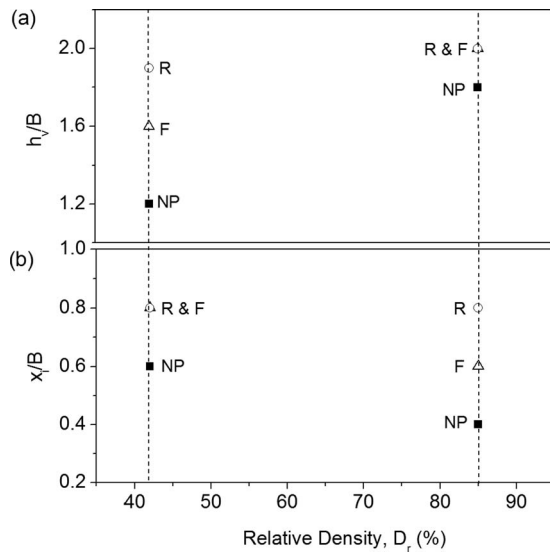


Fig. 12. Characteristics of failure surfaces developed in models containing rigid and flexible pipes and models without pipes: (a) height of the failure surface (h_v); (b) lateral extent of the failure surface (x_i)

tained in models without pipes, the failure patterns in transverse Sections S1 and S2 were very similar. However, the failure patterns observed in transverse Section S3 differed significantly from those recorded in the other two sections. h_v/B values in transverse Section S3 are 15–30% smaller than those recorded in transverse Sections S1 and S2. The only exception to that tendency was observed with Model D4 (flexible pipe in loose backfill), which showed a pattern in S3 more similar to that of transverse Sections S1 and S2. As previously discussed, less developed surfaces occur at the corners of the trapdoor due to the friction mobilized between the sliding soil mass above the trapdoor and the surrounding stable soil beyond the trapdoor. However, in the case of Model D4, the combination of a low shear strength (loose soil) and a low pipe stiffness resulted in the development of more homogeneous failure patterns across the entire pipe axis.

Inclusions have been reported to affect the development of failure surfaces within the soil mass. For example, biaxial compression tests reported by Vardoulakis and Graf (1985) involving cylindrical inclusions in a granular soil showed that the inclusion influences the failure surfaces as they start propagating around it. In this study, the presence of the pipe was found to significantly influence the pattern of the failure surfaces. Figs. 12(a and b) show values of h_v/B and x_i/B obtained in transverse Section S1 for different backfill relative densities (D_r) in models involving flexible (F) pipes, rigid (R) pipes, and no pipes (NP). The presence of the pipe led to better developed failure zones than in the cases without pipes, as shown in the figure by the values of h_v/B and x_i/B . The lateral spread of the failure zone (larger x_i) is more significant in models with dense backfill. Since the soil column over the pipe is prevented from sliding directly into the void, the unstable soil mass spreads laterally into the zone adjacent to the trapdoor in order to fill the void. Without the pipe, the soil does not find obstacles and the unstable zone concentrates more over the trapdoor.

The results in Fig. 12 also show that the presence of rigid (R) pipes resulted in larger failure zones than the presence of flexible (F) pipes, in both dense and loose backfills. While x_i/B was more influenced by pipe stiffness in dense backfills, h_v/B was more influenced by pipe stiffness in loose backfills. The compatibility

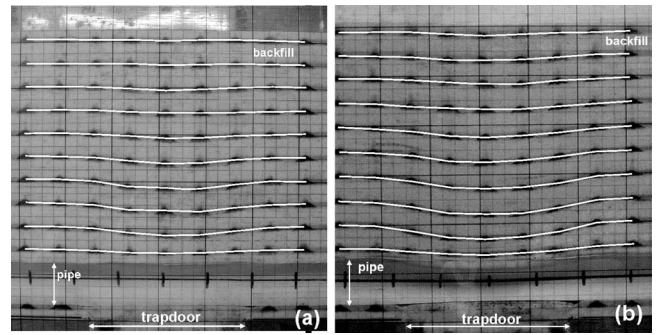


Fig. 13. Subsidence pattern on the longitudinal section: (a) Model D3 (flexible pipe in dense backfill); (b) Model D4 (flexible pipe in loose backfill)

between the deformations of the pipe and the surrounding soil is larger for flexible pipes than for rigid pipes. As a result, smaller failure zones are obtained with flexible pipes. Particularly, the influence of pipe stiffness was more significant on the development of the innermost failure surface.

Table 7 summarizes the surficial settlement values ($s_{0.25}/\delta$) obtained on transverse Section S1 of the models containing pipes (Models D1 to D4). It is noted that the presence of the pipe appears not to influence significantly the recorded surficial settlement. Consistent with the trend observed in series without pipes, surficial settlements were approximately three times larger in models with loose backfill than in models with dense backfill.

Well-defined failure surfaces did not develop in the longitudinal direction of the models (y - z plane). Instead, zones of subsidence were observed in the soil mass due to the migration of sand into the void. The failure patterns in the longitudinal direction for Models D3 and D4 (flexible pipes in dense and loose backfills) are shown in Figs. 13(a and b), respectively. The extent of the failure zone in the longitudinal direction was quantified by parameter y_i , which is the maximum horizontal length of the surface measured from the corner of the trapdoor. In the models with loose backfill, y_i/B equals 0.4 with flexible pipe and 0.25 with rigid pipe. On the other hand, y_i/B was found to be negligible in models with dense backfill, regardless the pipe stiffness. Inspection of Figs. 13(a and b) shows that the zone of soil subsidence is more pronounced in models with loose backfill, which is consistent with the trend of surficial settlements as shown in Table 7. It should also be noted that the larger settlements in the soil mass did not take place immediately over the pipe, but at an elevation of approximately one pipe diameter over the pipe crown.

The results from Models D3 and D4 provide additional insight into the performance of buried flexible pipes, which need to strongly interact with the surrounding soil. Under loading, flexible buried pipes deflect and adopt an elliptical shape. Passive resistance is thus mobilized at the lateral sides of the pipe, limiting the horizontal deflections and increasing the pipe load-carrying capacity. Therefore, proper compaction of the soil at the sides of the pipe will significantly improve its performance.

Proper backfill compaction is also relevant for the case of pipes undergoing a localized loss of ground support. In spite of the low stiffness of the flexible pipe embedded in the model with dense backfill (D3), only very small deformations were observed even after large trapdoor movements [Fig. 13(a)]. However, the performance of the flexible pipe embedded in the model with loose backfill (D4) was compromised after ground loss. Specifically, buckling occurred at the shoulder and the crown of the pipe,

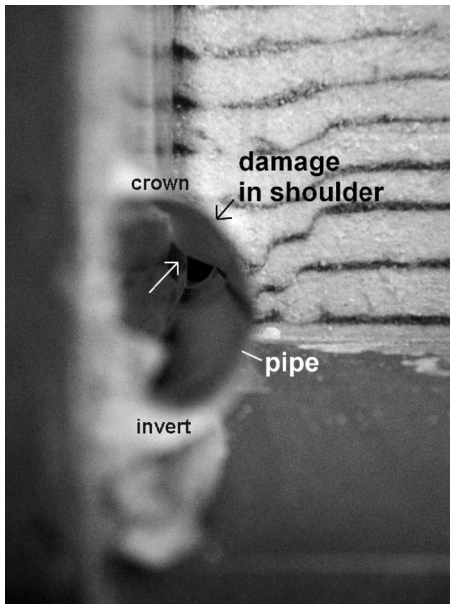


Fig. 14. Damage observed in Section S1 of Model D4 (flexible pipe in loose backfill)

and a reversal of curvature was noted at the invert due to overdeflection [Fig. 13(b)] In this model, the damage to the pipe after the localized loss of ground support was more critical in transverse Section S1, but was less severe toward the edges of the trapdoor. The damage to the shoulder of the pipe in transverse Section S1 of Model D4 is shown in Fig. 14.

The results obtained using the half sectioned pipes compare well with the results obtained from tests conducted using full sectioned pipes subjected to ground loss. Fig. 15 shows the results of a reduced-scale model test containing a whole sectioned pipe (with 75 mm in outside diameter and 2 mm in wall thickness) overlying a rectangular active trapdoor. The model represents an installation comprising a flexible pipe in loose backfill ($D_r = 50\%$). The general characteristics of the whole section model, including backfill soil conditions, model and trapdoor geometry,

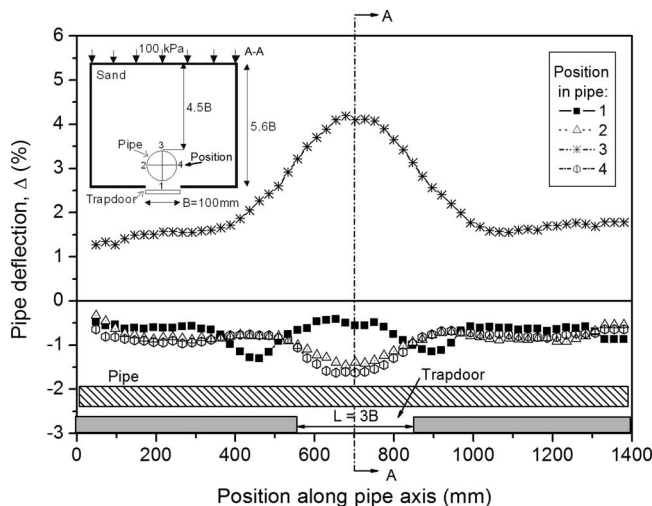


Fig. 15. Deflections measured along a whole sectioned flexible pipe in loose backfill ($D_r = 50\%$) overlying a rectangular active trapdoor ($\delta/B = 15\%$) (Costa 2005)

and pipe stiffness are consistent with those of the half sectioned reduced-scale models (Costa 2005). Although the stress field in the whole sectioned model was controlled using a pressurized bladder, the stress level in the trapdoor region was similar to that obtained in the centrifuge for the half sectioned pipes.

Fig. 15 shows the variation of the deflections (Δ) measured along pipe axis in four distinct positions (crown, invert, and spring-lines) for a relative displacement (δ/B) of 15%. Pipe deflection is presented in the figure as the measured displacement at the selected pipe position normalized with the pipe diameter. Negative values of Δ correspond to movements away from the pipe center. The deflections shown in Fig. 15 indicate that the whole sectioned pipe experienced buckling at the crown and a reversal of curvature at the invert due to overdeflection after ground loss. This trend was less severe toward the edge of the trapdoor. This response is consistent with that observed for the half sectioned flexible pipe embedded in loose backfill (Model D4).

Conclusions

Failure mechanisms in a granular soil induced by the active movement of a rigid trapdoor were evaluated in this study. An experimental program was conducted, which involved reduced-scale models tested under normal gravity as well as under 45 g using a centrifuge facility. The models were constructed with a soil cover of 4.5 times the width of the trapdoor, which correspond to deep conditions. Failure mechanisms obtained after the downward movement of the trapdoor were investigated in longitudinal and transverse sections of the models. Some models were used to evaluate the performance of buried pipes undergoing a localized loss of ground support.

The following conclusions can be drawn from the analysis of the data collected as part of this investigation:

- The failure mechanisms for active trapdoors under deep conditions differed significantly from those observed under shallow conditions. The mechanisms reported for shallow conditions involve the development of multiple failure surfaces in the region above the trapdoor (i.e., internal failure surfaces), with soil directly above the trapdoor remaining essentially rigid. Instead, the failure mechanism observed in this study for deep conditions involved the development of a single, well-defined internal failure surface which becomes gradually more inclined to the vertical for increasing downward trapdoor movement.
- As quantified by strain fields obtained from photographic monitoring of the models, the soil directly above the trapdoor showed significant dilation in the direction of the trapdoor movement.
- Assessment of the failure mechanisms in the transverse direction of the models indicated the development of multiple failure surfaces extending outside the limits of the trapdoor. Failure zones with heights ranging from 1.2 to nearly twice the trapdoor width and lateral extensions ranging from 1.4 to over twice the trapdoor width were obtained for large trapdoor displacements.
- The pattern of the failure surfaces induced by active trapdoor movements was significantly influenced by the stress level. High stress levels led to better defined failure zones.
- The soil relative density (D_r) influenced significantly the magnitude of the surficial settlements. Surficial settlements as large as approximately 15% of the imposed trapdoor displacement

were obtained in loose backfills. In general, surficial settlements were approximately three times larger in loose backfills than in dense backfills. These results provide insight into the magnitude of differential settlements that structures at the ground surface may undergo due to the construction of deep underground structures.

- The presence of inclusions, such as pipes, directly above the active trapdoor affects significantly the development of failure surfaces. Specifically, the presence of pipes resulted in larger failure zones as compared to those obtained in models without pipes. Failure involved multiple failure surfaces extending outside the trapdoor limits, to a maximum distance of 0.8 times the trapdoor width (B) and to a maximum height of twice the trapdoor width. The extent of the failure zone was observed to decrease with increasing pipe stiffness.
- The soil density influences significantly the performance of flexible pipes undergoing localized loss of ground support. Pipes embedded in loose backfill experienced significant damage after ground loss, which was characterized by severe buckling in the region between the shoulder and the crown and by a reversal of curvature at the invert due to overdeflection. On the other hand, the pipes embedded in dense backfill suffered negligible deflections after ground loss of support. These results indicate that damage to pipelines caused by ground loss can be significantly minimized by controlling the compaction of the fill.

Acknowledgments

The writers are grateful to the Brazilian research agency FAPESP for the financial support provided to this research and to the Civil Engineering Department of the University of Colorado at Boulder for the access to the centrifuge facilities.

References

- Batiste, S. N. (1998). "Mechanics of granular materials at low confining stress." MS thesis, Univ. of Colorado at Boulder.
- Bolton, M. D. (1986). "The strength and dilatancy of sands." *Geotechnique*, 36(1), 65–78.
- Costa, Y. D. J. (2005). "Physical modeling of buried pipes subjected to localized loss of support or elevation." Ph.D. thesis, School of Engineering of São Carlos, Univ. of São Paulo, Brazil (in Portuguese).
- Evans, C. H. (1983). "An examination of arching in granular soils." MS thesis, Department of Civil Engineering, MIT.
- Hartley, S. (1982). "Shear bands in sand. Part II." *Project Rep.*, Dept of Engineering, Univ. of Cambridge, Cambridge, U.K.
- Katona, M. G. (1988). "Allowable fill height for corrugated polyethylene pipe." *TRB 1191*, Transportation Research Board, National Research Council, Washington, D.C.
- Ko, H. Y. (1988). "The Colorado centrifuge facility." *Proc., Centrifuge '88*, Balkema, Rotterdam, 73–75.
- Koutsabeloulis, N. C., and Griffiths, D. V. (1989). "Numerical modeling of the trap door problem." *Geotechnique*, 39(1), 77–89.
- Ladanyi, B., and Hoyaux, B. (1969). "A study of the trap-door problem in a granular mass." *Can. Geotech. J.*, 6(1), 1–15.
- McNulty, J. W. (1965). "An experimental study of arching on sand." *Technical Rep. No. I-674*, U.S. Waterways Experimental Station, Vicksburg.
- Muir Wood, D. (2002). "Some observations of volumetric instabilities in soils." *Int. J. Solids Struct.*, 39, 3429–3449.
- Ono, K., and Yamada, M. (1993). "Analysis of the arching action in granular mass." *Geotechnique*, 43(1), 105–120.
- Peck, R. B. (1969). "State-of-the-art report: Deep excavations and tunneling in soft ground." *Proc., 7th Int. Conf. in Soil Mechanics and Foundation Engineering*, Mexico City, 225–290.
- Roscoe, K. H. (1970). "The influence of strains in soil mechanics." *Géotechnique*, 20(2), 129–170.
- Santichaiant, K. (2002). "Centrifuge modeling and analysis of active trapdoor in sand." Ph.D. thesis. Dept. of Civil, Environmental and Architectural Engineering, Univ. of Colorado at Boulder.
- Scarpelli, G. (1981). "Shear bands in sands." MPhil thesis, Univ. of Cambridge, Cambridge, U.K.
- Sloan, S. W., Assadi, A., and Purushothaman, N. (1990). "Undrained stability of a trapdoor." *Geotechnique*, 40(1), 45–62.
- Stone, K. J. L., and Muir Wood, D. (1992). "Effects of dilatancy and particle size observed in model tests on sand." *Soils Found.*, 32(4), 43–57.
- Tanaka, T., and Sakai, T. (1993). "Progressive failure and scale effect of trap-door problems with granular materials." *Soils Found.*, 33(1), 11–22.
- Terzaghi, K. (1936). "Stress distribution in dry and saturated sand above a yielding trap-door." *Proc., 1st International Conference on Soil Mechanics and Foundation Engineering*, Cambridge, Mass., 35–39.
- Terzaghi, K. (1943). *Theoretical soil mechanics*, Wiley, New York.
- Vardoulakis, I., and Graf, B. (1985). "Calibration of constitutive models for granular materials using data from biaxial experiments." *Geotechnique*, 35(3), 299–317.
- Vardoulakis, I., Graf, B., and Gudehus, G. (1981). "Trap-door problem with dry sand: A statical approach based upon model kinematics." *Int. J. for Numerical and Analytical Methods in Geomechanics*, 5, 57–78.
- Yimsiri, S., Soga, K., Yoshizaki, K., Dasari, G., and O'Rourke, T. (2004). "Lateral and upward soil-pipeline interactions in sand for deep embedment conditions." *J. Geotech. Geoenviron. Eng.*, 130(8), 830–842.
- Zornberg, J. G., and Arriaga, F. (2003). "Strain distribution within geosynthetic-reinforced slopes." *J. Geotech. Geoenviron. Eng.*, 129(1), 32–45.
- Zornberg, J. G., Sitar, N., and Mitchell, J. (1998). "Performance of geosynthetic reinforced slopes at failure." *J. Geotech. Geoenviron. Eng.*, 124(8), 670–683.